Supplementary Materials

Amalgamation of $MnWO_4$ nanorods with amorphous carbon nanotubes for highly stabilized energy efficient supercapacitor electrode

Kausik Sardar[1], Subhasish Thakur[1], Soumen Maiti[2], Nripen Besra[3], Partha Bairi[3], Kausik Chanda[3], Gautam Majumdar [4], Kalyan Kumar Chattopadhyay[1,3] *

[1]*School of Materials Science and Nanotechnology, Jadavpur University, Kolkata 700032, India*

[2]*St Thomas College of Engineering & Technology, Kolkata 700023, India*

[3]*Department of Physics, Jadavpur University, Kolkata 700032, India*

[4]*Department of Mechanical Engineering, Jadavpur University, Kolkata 700032, India*

*Corresponding author E-mail: kalyan_chattopadhyay@yahoo.com

Electrode prepartaion

The working electrodes were prepared using of $MnWO_4$-aCNT, polytetrafluoroethylene (PVDF) and carbon black with a ratio of 8:1:1. The aforesaid reagents were mixed with 300 µL NMP and stirred for 6 hours to obtain a black paste. This mixture was coated on precleaned and dry Ni Foam and dried at 70 ˚C for 12 hours.

Characterizations

X-ray diffraction study was performed using X-ray diffractometer (Bruker D8: Advance). Morphology of the products was examined by field emission scanning electron microscope (FESEM, Hitachi S-4800). EDS study was performed using energy dispersive spectroscopy (EDS, Thermo Scientific attached with the FESEM). To get more details about morphology and crystal structure transmission electron microscope (JEOL, JEM 2100) study was further performed. Raman spectra were recorded using Raman spectrometer (alpha 300, Witec). BET

measurements were carried out using Nova 1000e, Quantachrome. Electrochemical tests were studied in Gamry Interface 1000 (potentiostat/galvanostat/ZRA).

Electrolyte gel preparation for ASC device

For the preparation of electrolyte gel, PVA, KOH and DI water was used. A mixture of PVA, KOH and DI water was stirred vigorously. Mixture temperature was maintained at 90 ºC and the solution was stirred until the solution became transparent and homogeneous. After the gel formation, it was cooled to room temperature which eliminated the as formed excess bubbles.

Table S1:

Sample	Scan rate (mVs^{-1})	Specific capacitance (Fg^{-1})
aCNT	5	113.86
	10	76.34
	20	52.18
	50	31.27
	75	24.31
	100	20.35
$MnWO_4$	2	231.15
	5	196.13
	10	166.58
	20	139.72
	50	102.38
	75	85.43
	100	73.88
$MnWO_4$-aCNT	2	542.18
	5	388.81
	10	298.95
	20	233.88
	50	157.94
	75	130.04
	100	112.52

Table S2: Values of equivalent circuit components.

Component	Value	
	$MnWO_4$-aCNT	$MnWO_4$
R_1 (ohm)	0.3265	0.9711
R_2 (ohm)	1.434	2.033
R_3 (ohm)	0.5731	0.7835
W_1 (ohm $S^{-1/2}$)	11.13	28.7
W_2 (ohm $S^{-1/2}$)	0.7003	0.9812
C_1 (F)	0.162×10^{-3}	0.6021×10^{-24}
C_2 (F)	8.366×10^{-3}	2.479×10^{-3}
C_3 (F)	3.039	1.121

Table S3: Electrochemical performance comparison:

Electrode material	Electrolyte	Specific capacitance	Potential window	Energy density	Cycling stability	Ref.
SWCNT	KOH + p-phenylenediamine	162.66 Fg^{-1} at 1 Ag^{-1}	-0.8 to 0.2 V	4.23 W h kg^{-1}	96.51% after 4000 cycles	1
MWCNTs	KOH + m-phenylenediamine	78 Fg^{-1} at 0.5 Ag^{-1}	-0.5 to 0.5 V	9.99 W h kg^{-1}	90.68% after 10000 cycles	2
MWCNTs	H_2SO_4 + indigo carmine	50 Fg^{-1} at 0.88 mA cm^{-2}	0 to 1 V	1.7 W h kg^{-1}	30% after 10000 cycles	3
NGPC15	KOH	227.9 Fg^{-1} at 2 mV s^{-1}	-1 to 0 V	-	106% after 5000 cycles	4
Boron-doped carbon	H_2SO_4	228 Fg^{-1} at 1 mV s^{-1}	0 to 1 V	8.65 W h kg^{-1}	100% after 1000 cycles	5
Carbon nanotube	KOH	180 Fg^{-1}	0 to 0.9 V	6.5 W h kg^{-1}	-	6
N_2-doped carbon nanofibers	KOH	202 Fg^{-1} at 1 Ag^{-1}	-1 to 0 V	7.11 W h kg^{-1}	97% after 3000 cycles	7
Mesoporous carbon	KOH	128 Fg^{-1} at 50 mA g^{-1}	0.2 to 1 V	1.16 W h kg^{-1}	-	8
Mesoporous fullerene	KOH	172 Fg^{-1} at 0.5 Ag^{-1}	-1 to 0 V	-	Significant drop after 1000 cycles	9
TiO_2 anchored to CNT	KOH	130.4 Fg^{-1} at 1 Ag^{-1}	-0.05 to 0.5 V	4.47 W h kg^{-1}		10
$MnWO_4$/RGO	KOH	288 Fg^{-1} at 5 mV s^{-1}	-0.35 to 0.55 V	-	14.9% after 6000 cycles	11
$MnWO_4$	Na_2SO_4	386 Fg^{-1} at 5 mVs^{-1}	0 to 1 V	-	90% after 2000 cycles	12
$MnWO_4$	KOH	295 Fg^{-1} at 5 mVs^{-1}	-0.2 to 0.6 V	16 Wh kg^{-1}	> 100% after 3000 cycles	13
WO_3-RGO composite	H_2SO_4	495 Fg^{-1} at 1 Ag^{-1}	-0.4 to 0.3 V	-	87.5% after 1000 cycles	14
$MnWO_4$ micro flower	Na_2SO_4	324 Fg^{-1} at 1 mA cm^{-2}	0 to 1 V	34 W h kg^{-1}	93% after 8000	15
$MnWO_4$@ aCNT	**KOH**	**542.18 Fg^{-1} at 2 mVs^{-1}**	**-0.1 to 0.6 V**	**5.6 W h kg^{-1}**	**Above 100% after 15,000 cycles**	**This work**

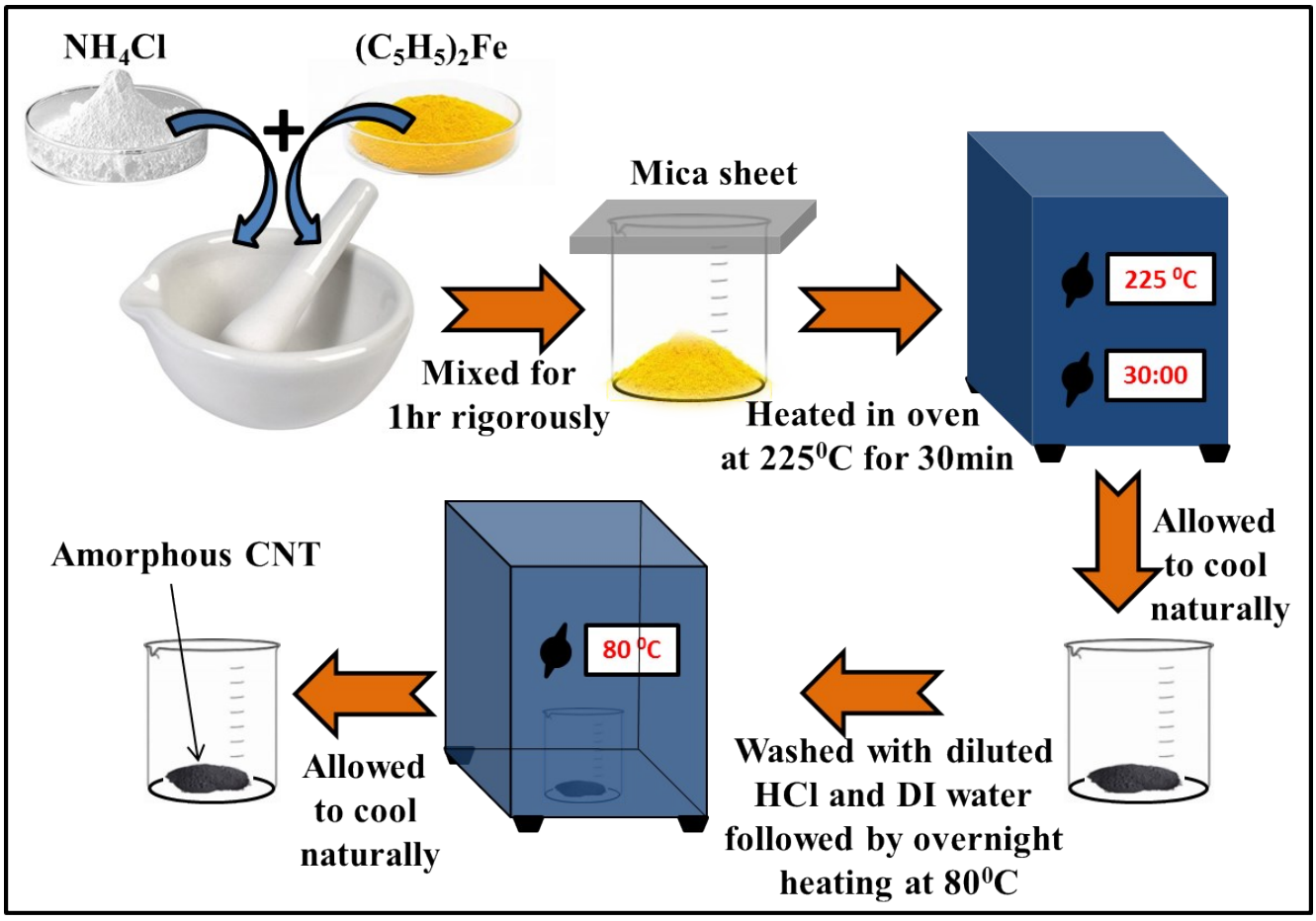

Figure S1: Schematic of synthesis protocol of aCNT.

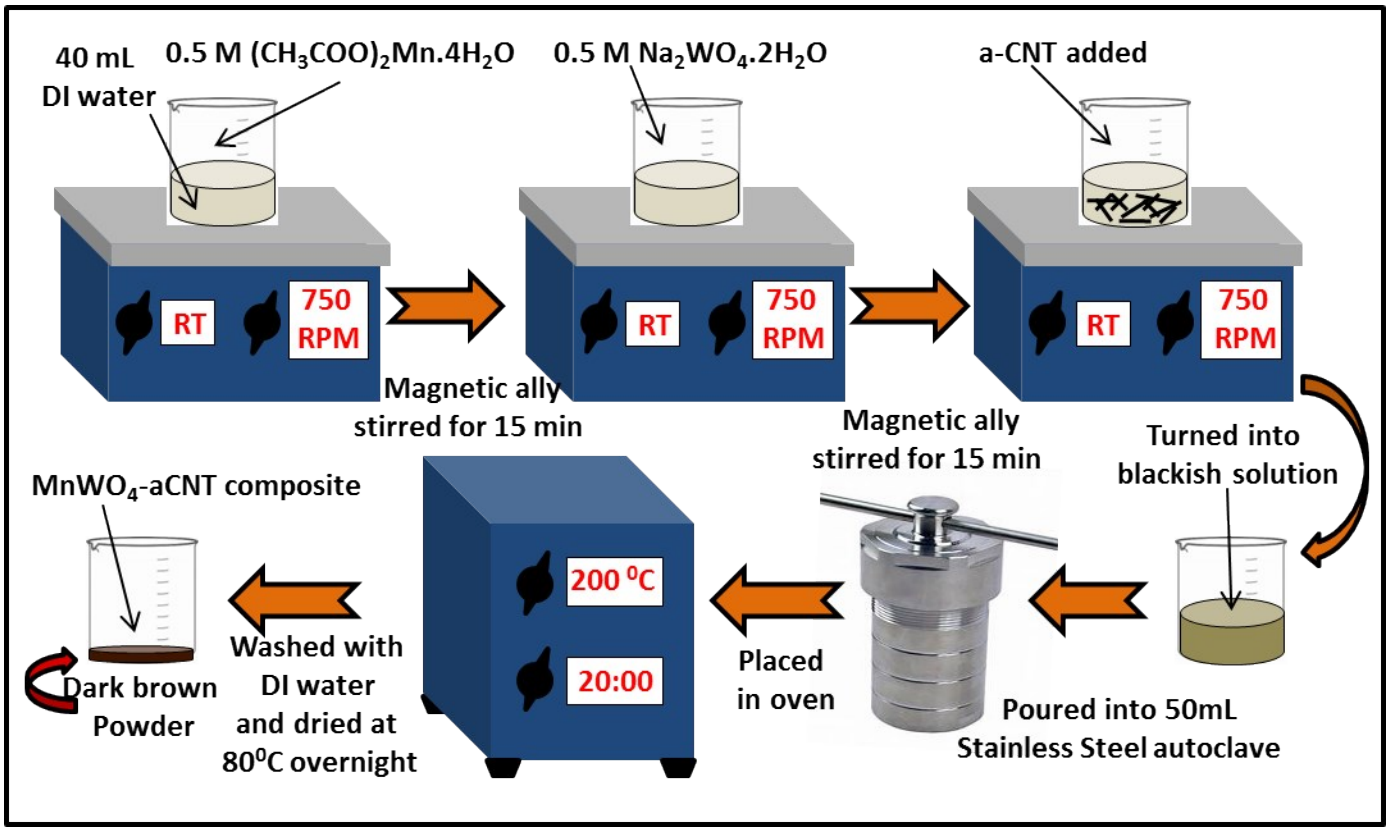

Figure S2: Schematic of synthesis protocol of $MnWO_4$-aCNT hybrid.

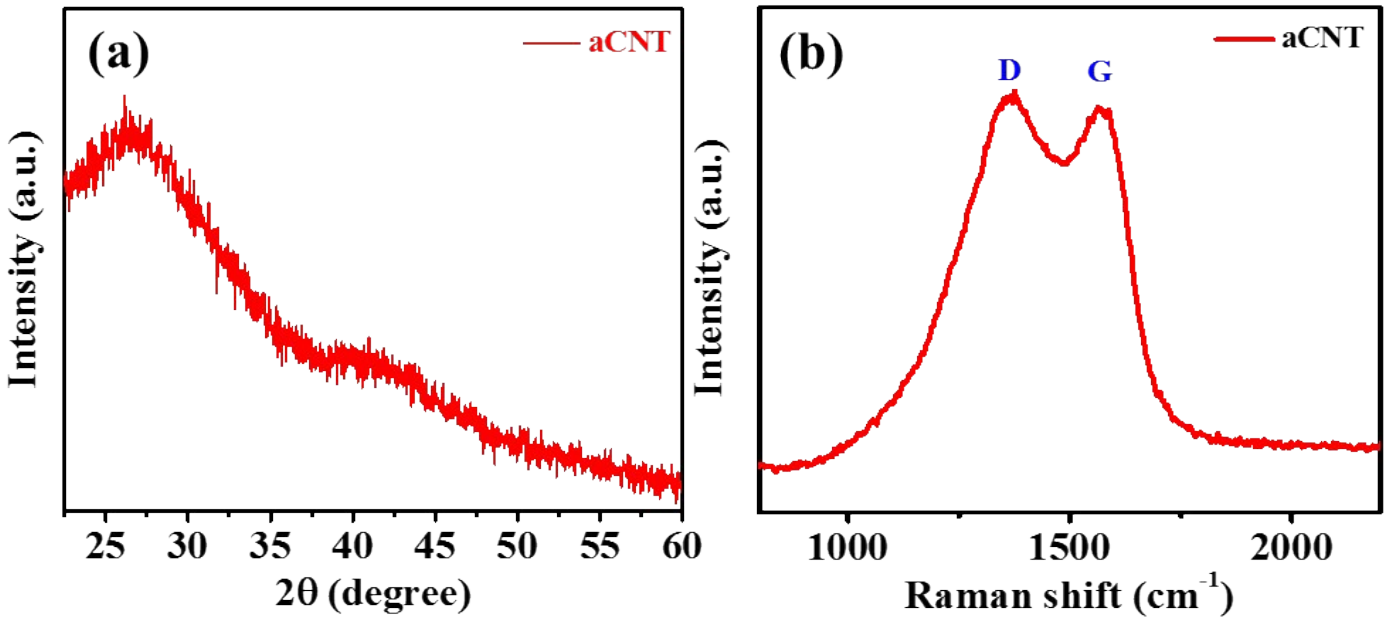

Figure S3: (a) XRD and (b) RAMAN spectra of aCNT.

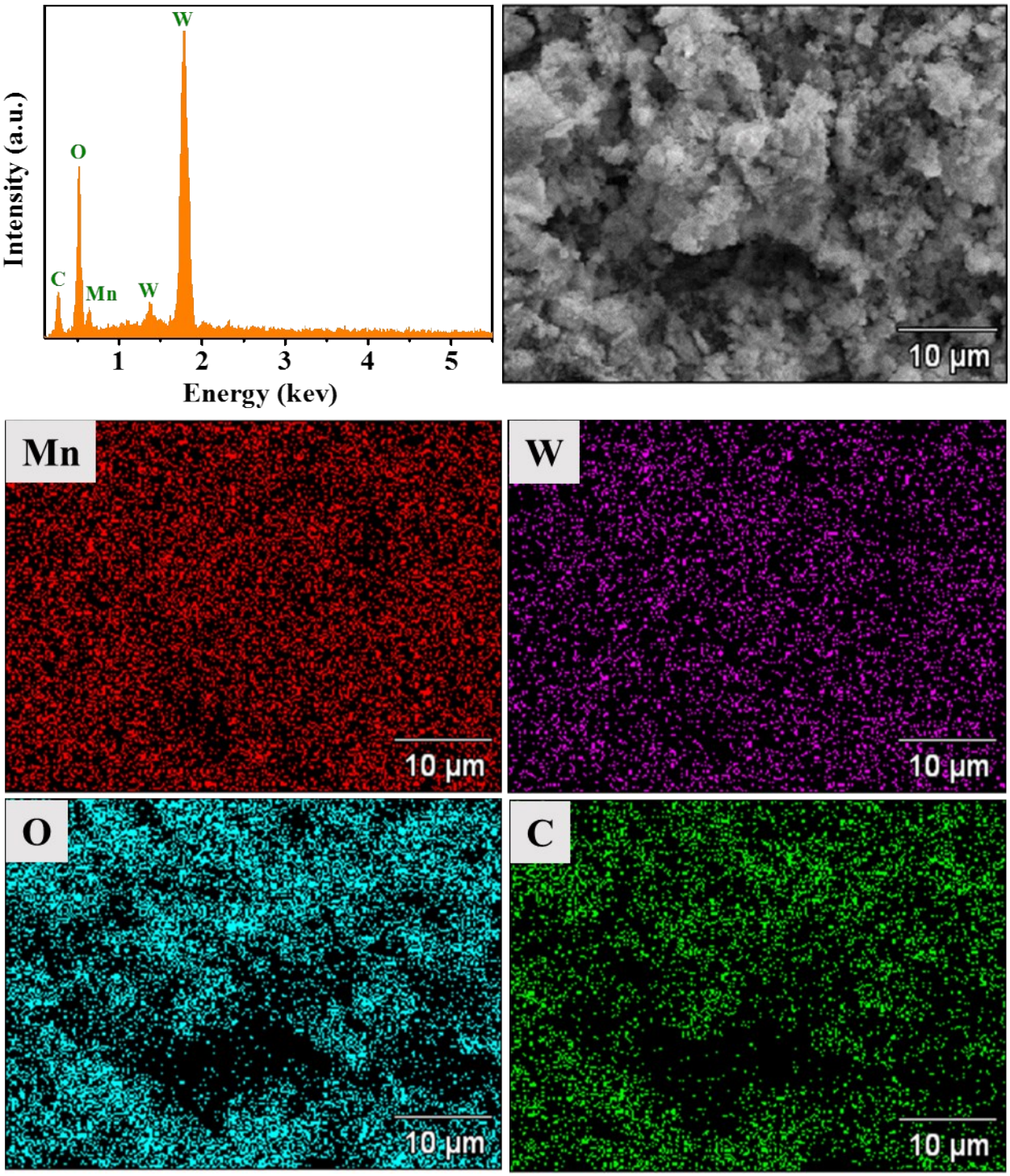

Figure S4: EDS spectrum and associated elemental mapping of $MnWO_4$-aCNT.

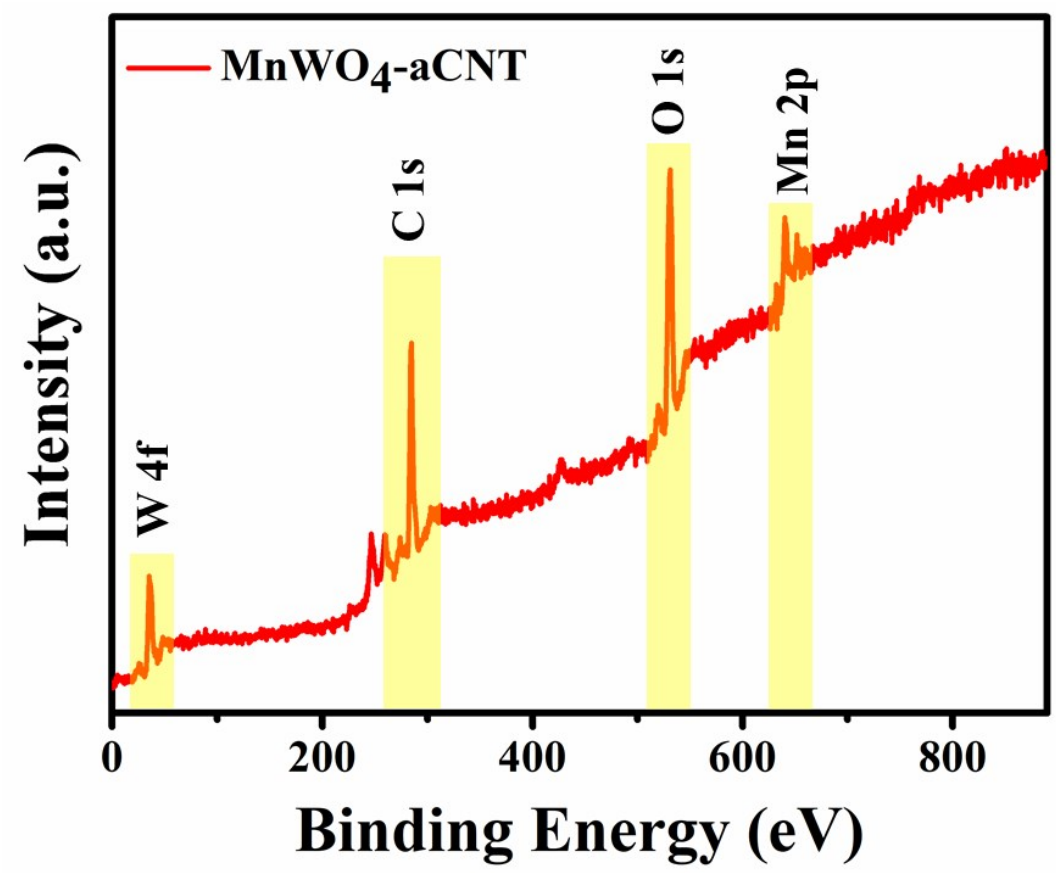

Figure S5: XPS survey scan of $MnWO_4$-aCNT.

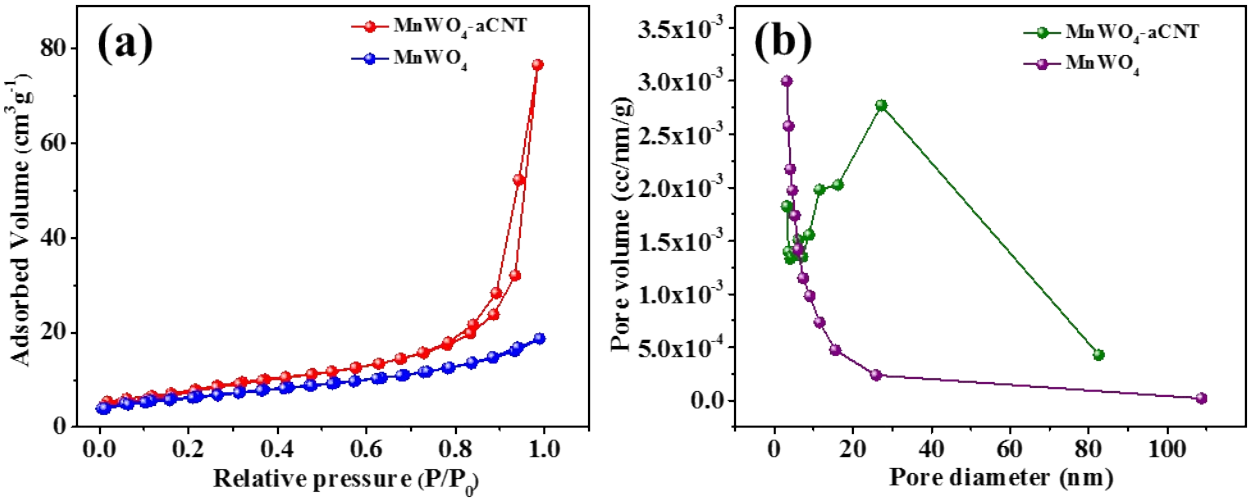

Figure S6: (a) N_2 adsorption–desorption isotherms and (b) pore distributions of $MnWO_4$-aCNT and $MnWO_4$.

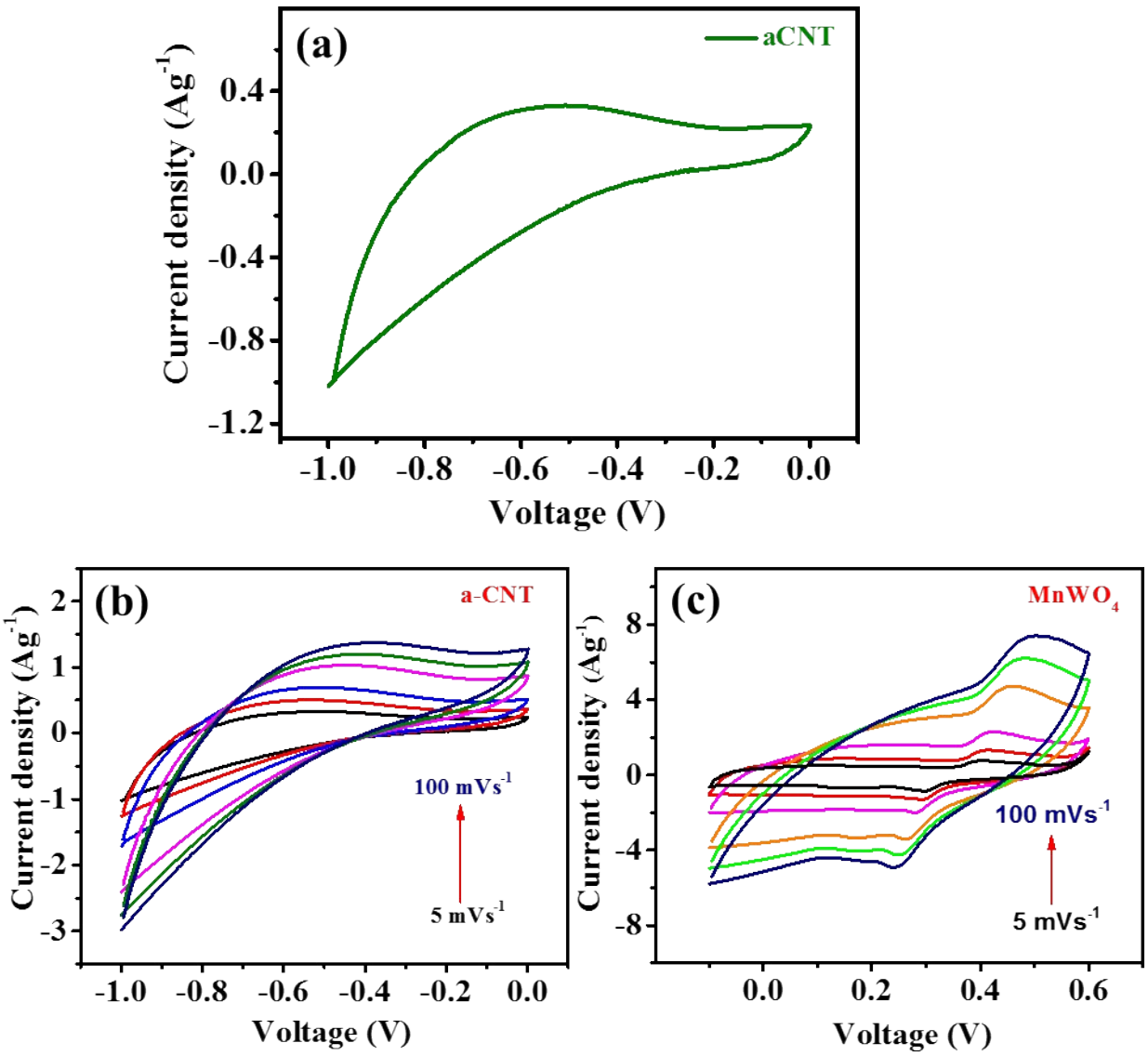

Figure S7: CV curves of (a) aCNT at 5mVs^{-1}; (b) aCNT and (b) $MnWO_4$ at different scan rates.

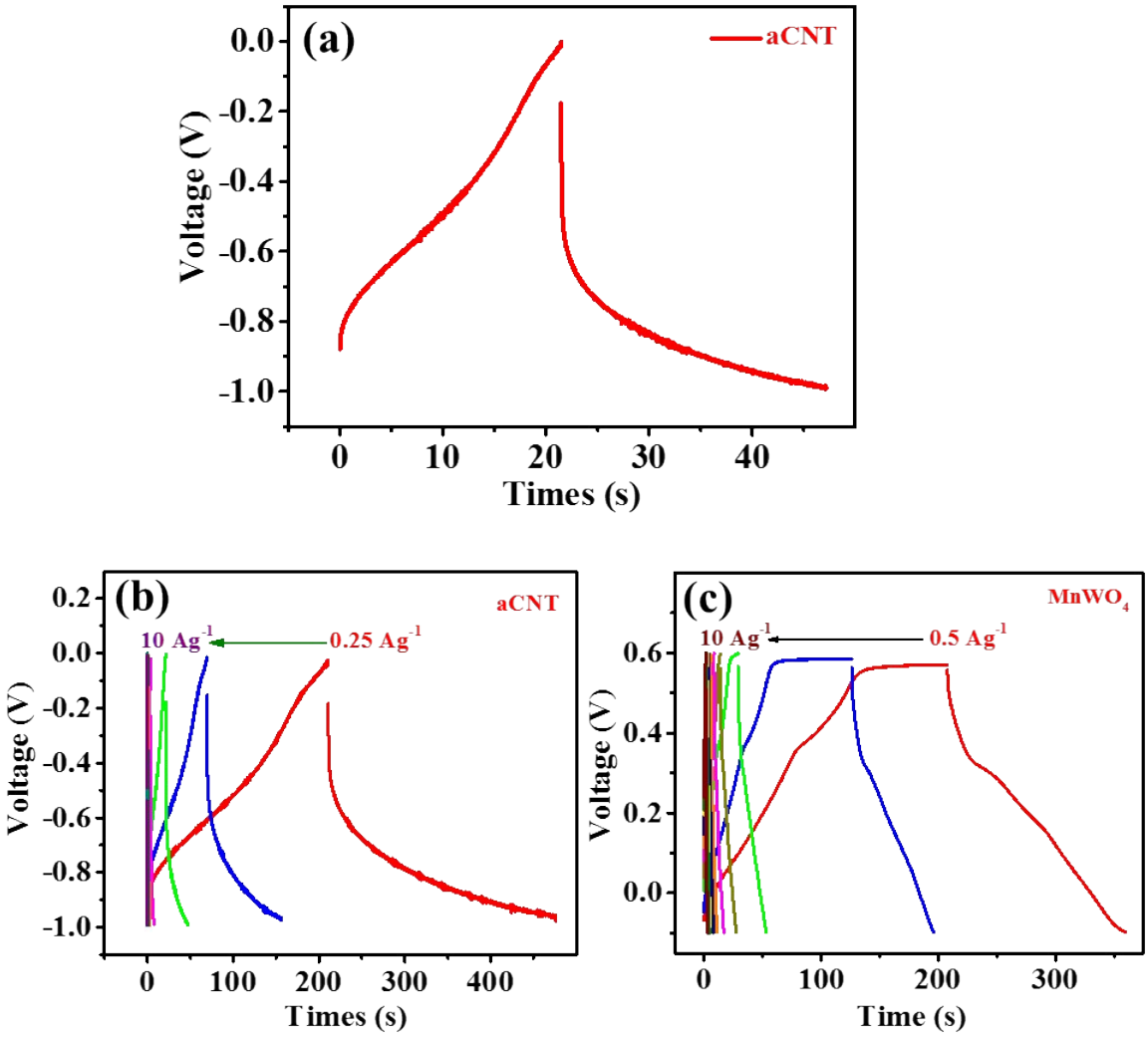

Figure S8: GCD curves of (a) aCNT at 1 Ag^{-1}; (b) aCNT and (c) $MnWO_4$ at different current density.

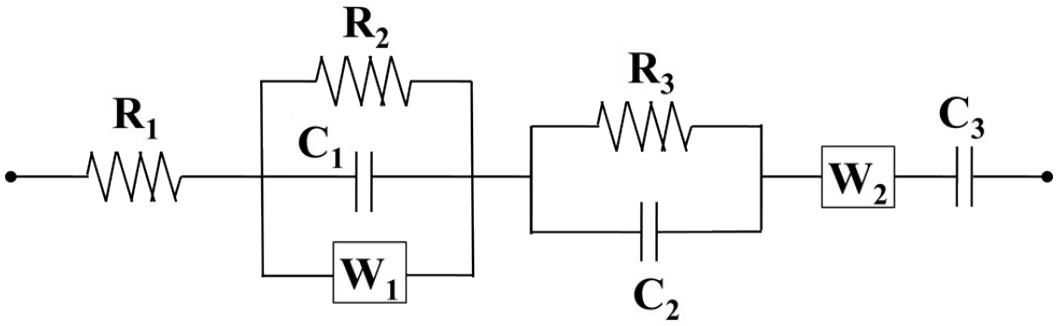

Figure S9: Equivalent circuit which is used to fit the EIS spectra.

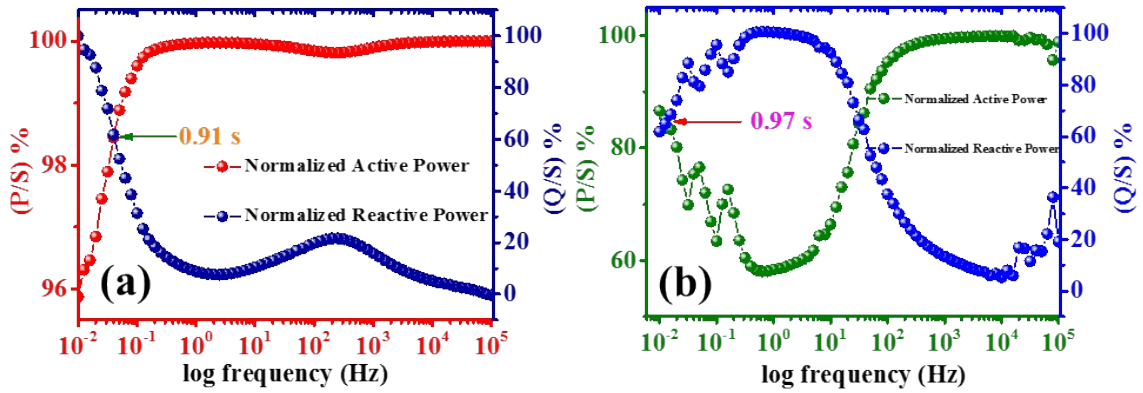

Figure S10: Active power and reactive power of (a) $MnWO_4$-aCNT and (b) $MnWO_4$.

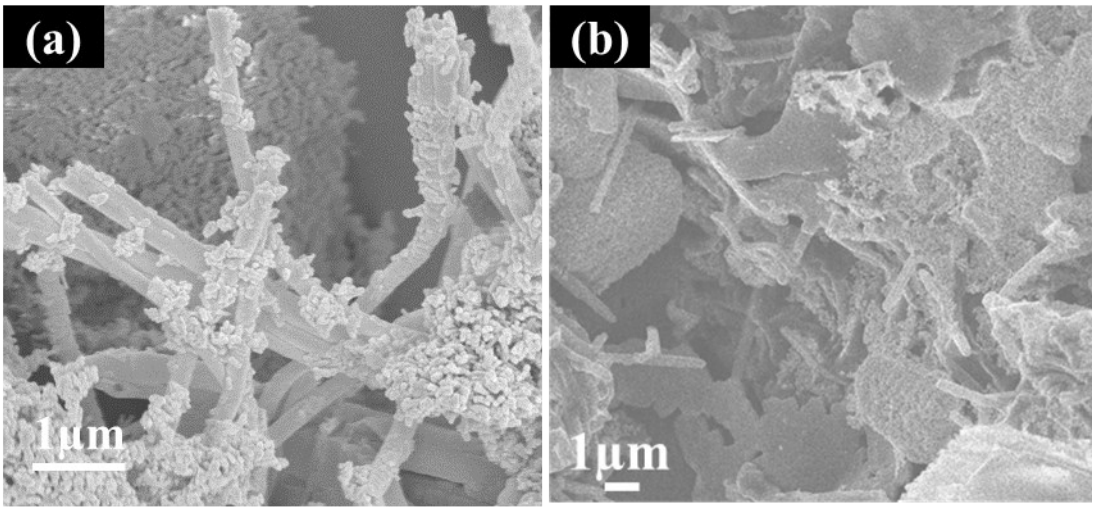

Figure S11: FESEM image of the hybrid before and after 15000 cycles.

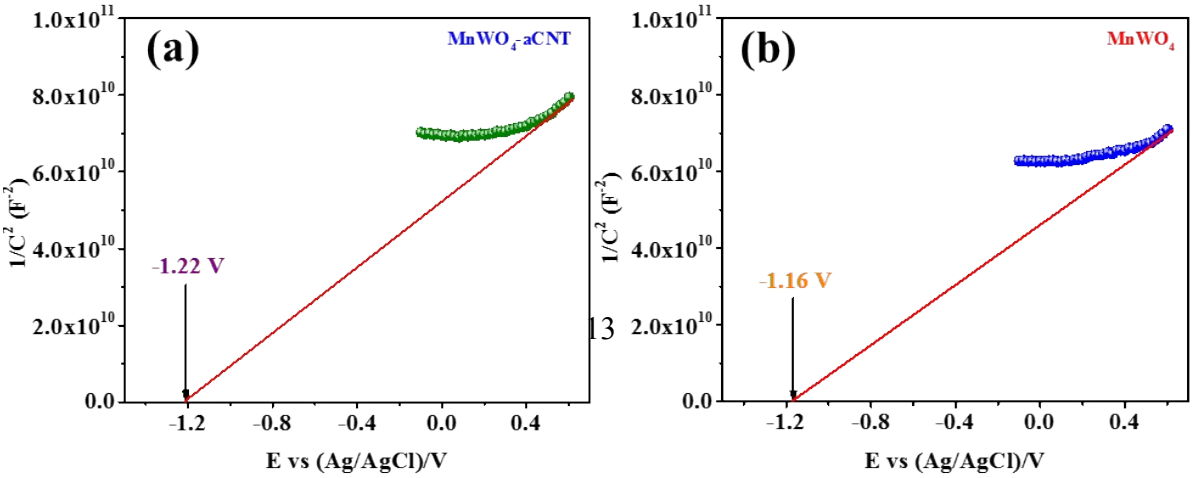

Figure S12: Mott Schottky plot of the (a) $MnWO_4$-aCNT and (b) $MnWO_4$.

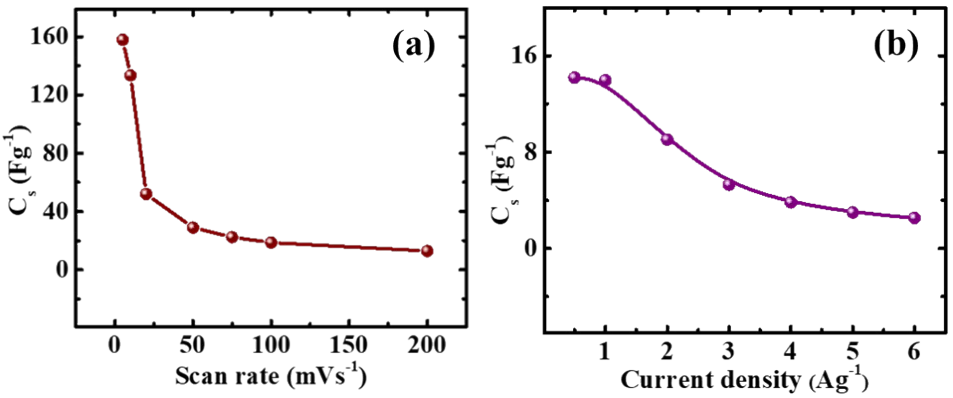

Figure S13: Variation in C_s of ASC with respect to (a) scan rate (b) current density.

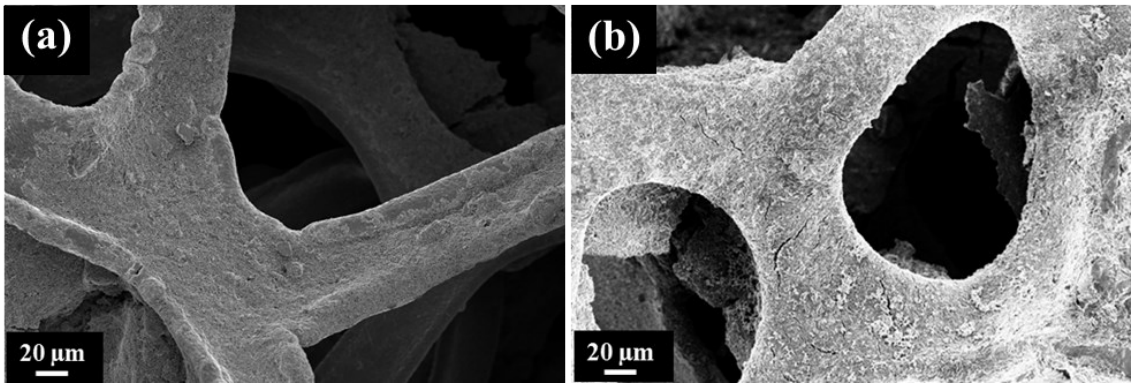

Figure S14: FESEM image of the nickel foam (a) before and (b) after 6000 cycles operation.

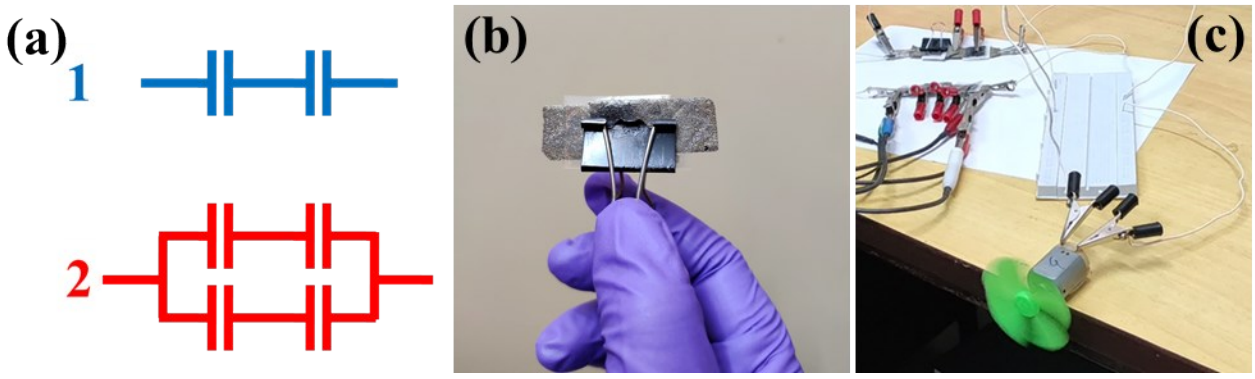

Figure S15: (a) **ASC** Device arrangement in series and series/parallel; (b) single ASC Device and (c) digital photographs of running motor fan.

Reference:

1. H. Yu, J. Wu, J. Lin, L. Fan, M. Huang, Y. Lin, Y. Li, F. Yu, and Z. Qiu, *ChemPhysChem*, 2013, **14**, 394-399.
2. H. Yu, L. Fan, J. Wu, Y. Lin, M. Huang, J. Lin, and Z. Lan, *RSC Adv.*, 2012, **2**, 6736-6740.
3. S. Roldán, Z. González, C. Blanco, M. Granda, R. Menéndez, and R. Santamaría, *Electrochim. Acta*, 2011, **56**, 3401-3405.
4. P. Bairi, K. Sardar, K. Chanda, M. Samanta, S. Thakur, K. Panigrahi, S. Sarkar, T. Paul, and K. K. Chattopadhyay, *ACS Appl. Energy Mater.*, 2020, **3**, 5984-5992.
5. Z. S. Wu, A. Winter, L. Chen, Y. Sun, A. Turchanin, X. Feng, and K. Müllen, *Adv. Mater.*, 2012, **24**, 5130-5135.
6. K. H. An, W. S. Kim, Y. S. Park, Y. C. Choi, S. M. Lee, D. C. Chung, D. J. Bae, S. C. Lim, and Y. H. Lee, *Adv. Mater.*, 2001, **13**, 497-500.
7. L. F. Chen, X. D. Zhang, H. W. Liang, M. Kong, Q. F. Guan, P. Chen, Z. Y. Wu, and S. H. Yu, *ACS nano*, 2012, **6**, 7092-7102.
8. S. R. S. Prabaharan, R. Vimala, and Z. Zainal, *J. Power Sources.*, 2006, **161**, 730-736.
9. M. R. Benzigar, S. Joseph, A. V. Baskar, D. H. Park, G. Chandra, S. Umapathy, S. N. Talapaneni, and A. Vinu, *Adv. Funct. Mater.*, 2018, **28**, 1803701.

10. X. Sun, M. Xie, J. J. Travis, G. Wang, H. Sun, J. Lian, and S. M. George, *J. Phys. Chem. C*, 2013, **117**, 22497-22508.
11. J. Tang, J. Shen, N. Li, and M. Ye, *J. Alloys Compd.*, 2016, **666**, 15-22.
12. J. Yesuraj, E. Elanthamilan, B. Muthuraaman, S. A. Suthanthiraraj, and J. P. Merlin, *J. Electron. Mater.*, 2019, **48**, 7239-7249.
13. F. Li, X. Xu, J. Huo, and W. Wang, *Mater. Chem. Phys.*, 2015, **167**, 22-27.
14. J. Chu, D. Lu, X. Wang, X. Wang, and S. Xiong, *J. Alloys Compd.*, 2017, **702**, 568-572.
15. B. G. S. Raj, J. Acharya, M. K. Seo, M. S. Khil, H. Y. Kim, and B. S. Kim, *Int. J. Hydrog. Energy*, 2019, **44**, 10838-10851.